



Investigation on surface integrity and process parameter optimisation of carburised 18CrNiMo7-6 steel by induction-heating-assisted ultrasonic surface rolling process

Zhihua Liu^{1,2} · Lingshuo Zheng^{1,2} · Peng Tang^{1,2} · Shengwei Qin^{1,2}

Received: 9 March 2023 / Accepted: 6 September 2023 / Published online: 26 September 2023
© The Author(s), under exclusive licence to Springer-Verlag London Ltd., part of Springer Nature 2023

Abstract

The purpose of induction-heating-assisted ultrasonic surface rolling process is to introduce the temperature field into the ultrasonic surface strengthening process of materials and use the influence of heating temperature on the mechanical properties and microstructure of the material so that a surface-modified layer with improved performance can be obtained. Many studies on the ultrasonic surface rolling process have been conducted at room temperature. In this study, the effect of temperature on the surface integrity of carburised 18CrNiMo7-6 steel after ultrasonic surface rolling process was studied by induction heating. Compared with the result of ultrasonic surface rolling process at room temperature, below 250 °C, with the increase of heating temperature, the residual compressive stress and residual compressive stress depth of the sample increase continuously. The maximum surface residual compressive stress and residual compressive stress depth can be obtained at 250 °C, the surface residual compressive stress increases by 29%, and the residual compressive stress depth increases from 1700 to 2450 µm. The surface hardness of the sample also shows an increasing trend when the heating temperature is from 100 to 250 °C, and the hardness influence layer increases with the increase of heating temperature. The minimum surface roughness can be obtained by ultrasonic surface rolling process at 100 °C. In addition, the induction-heating-assisted ultrasonic surface rolling process parameters are optimised by grey correlation analysis method, and the optimum process parameters to achieve the best surface integrity are obtained as follows: static pressure of 400 N, rotation speed of 50 r/min, feed rate of 0.04 mm/r, and heating temperature of 250 °C. The order of significance of influence on surface integrity is static pressure > rotation speed > feed rate > heating temperature. The conclusion has a certain guiding significance for the anti-fatigue manufacturing of materials.

Keywords Induction heating · Ultrasonic surface rolling process · Surface integrity · Carburised 18CrNiMo7-6 steel · Grey correlation analysis method · Parameter optimisation

1 Introduction

The working performance, reliability, and service life of mechanical equipment has attracted research attention [1–3]. How to increase the service life and decrease the fatigue failure of mechanical parts is particularly important. Surface

deformation strengthening can improve surface roughness, increase surface hardness, introduce residual compressive stress, and change the dislocation density of the material [4, 5], and is an effective method to improve surface properties. The commonly used methods of surface deformation strengthening are shot peening [6], laser shock strengthening [7], chemical heat treatment [8], rolling [9], and ultrasonic surface rolling process (USRP) [10–12]. Among these methods, USRP combines traditional rolling and ultrasonic vibration, which can improve the material microstructure, repair the disordered lattice arrangement, and realise the nanocrystallisation of the metal surface, thus greatly extending the fatigue life of the metal workpiece [13].

18CrNiMo7-6 alloy steel has good shock resistance and heat resistance, so it is the first choice for transmission gears

✉ Zhihua Liu
liuzhihua@zzu.edu.cn

¹ School of Mechanical and Power Engineering, Zhengzhou University, Zhengzhou 450001, Henan, China

² Henan Key Engineering Laboratory for Anti-Fatigue Manufacturing Technology, Zhengzhou 450001, Henan, China

and other key components in heavy machinery equipment [14]. After the carburising heat treatment, the surface of the 18CrNiMo7-6 alloy steel has high hardness and the core maintains the original toughness. This structure has been widely studied [15] because it improves the performance of the material and has broad application prospects in the key components of advanced engineering equipment. Through USRP technology, a deformation layer can be formed on the surface and the material properties can be further improved. However, the improvement of performance by USRP is limited because of low plasticity and high hardness on the surface of carburised steel. According to the research, heating can soften the material and increase the slip mechanism, thereby reducing the deformation energy required for severe plastic deformation of materials [16]. Induction-heating-assisted ultrasonic surface rolling process (IH-USRP) experiment is based on the normal USRP experiment, and the temperature field is introduced into the USRP strengthening process of the material. Under the influence of heating temperature, the surface of the material produces greater plastic deformation, thereby obtaining a better surface modification layer. Li et al. [17] studied the effect of different temperatures on the surface microstructure of USRP material and found that USRP at different temperatures can significantly increase the surface hardened layer depth and reduce the surface roughness. Zhang et al. [18] carried out heat-assisted ultrasonic burnishing on Fe-based laser cladding coating, and found that compared with ultrasonic burnishing at room temperature, the sample after heat-assisted ultrasonic burnishing has higher hardness, lower porosity, and better wear resistance. Juijerm et al. [19] studied the deep rolling to the aluminium alloy AA6110 fatigue behaviour effect at 160, 200, and 250 °C, and conclude that with the rolling temperature increases, the residual compressive stress decreases, and the hardness increases.

A reasonable heating method is necessary. During the IH-USRP, the heating temperature is required to be controllable and not too high, so as not to cause the structure change of the material; the heating layer depth is controllable and only the surface of the workpiece is heated without causing the overall heating; heating should be rapid to reduce the heating temperature to the initial residual stress state effect. In the current research on heating-assisted surface strengthening, the commonly used heating methods include laser heating [20], induction heating [21], and resistance wire heating [22]. Induction heating is a new method by which, through the principle of electromagnetic induction, eddy currents are generated inside the workpiece and their energy provides the heat. Induction heating has a skin effect, that is, the eddy current generated by the alternating magnetic field inside the heated workpiece is only scattered on the surface of the workpiece, but almost no eddy current occurs inside the workpiece. The higher the alternating magnetic field

frequency, the more obvious the skin effect and the shallower the heating depth. Compared with traditional heating methods, induction heating has the advantages of fast heating, energy saving, environmental protection, non-contact process, and strong controllability [23].

Various USRP parameters have different effects on the integrity of the sample surface. Hu et al. [24] carried out a USRP experiment on 60Si2CrVAT steel and found that as the static pressure increased, the residual compressive stress first increased and then decreased, and the hardness continued to increase. As rotation speed and feed rate increased, the hardness and residual compressive stress decreased, while the surface roughness increased. Mei et al. [25] provided a similar conclusion. Luan et al. [22] carried out USRP experiments at different temperatures and found that the surface roughness and residual compressive stress increased initially, and then decreased as the temperature increased. We hope that after the USRP experiment, the sample will have higher hardness and lower surface roughness while having larger residual compressive stress. The grey correlation analysis method can transform the multiple evaluation objectives comprehensive optimisation into the single grey correlation degree optimisation, and the grey correlation value is used to characterise the comprehensive performance of the system. Thus, the optimised parameter combination scheme is obtained [26], to investigate surface integrity of carburised 18CrNiMo7-6 steel after IH-USRP, and determine the heating temperature and USRP parameters. The effect of heating temperature was studied by combining theoretical analysis with experiments, and according to the grey correlation analysis method, the USRP parameters of carburised 18CrNiMo7-6 steel were optimised by orthogonal experiment. The optimal process parameters to achieve the best surface integrity and order of significance of various control factors to the effects of surface integrity were obtained.

2 Material and method

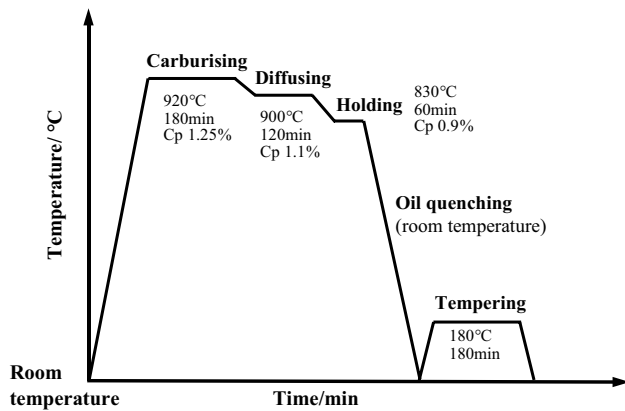
2.1 Material of workpiece

The material used in this study is 18CrNiMo7-6 alloy steel, which has high toughness and good comprehensive mechanical properties. Its main element composition is listed in Table 1 [15].

Carburising heat treatment is carried out on this material to study carburised 18CrNiMo7-6 steel. The specific carburising heat treatment process [27] is described as follows: methanol and isopropanol were used as the carburising agents. The sample was maintained for 180 min at 920 °C and 1.25% carbon potential for carburising. Then, heat preservation was carried out for 120 min at 900 °C and carbon

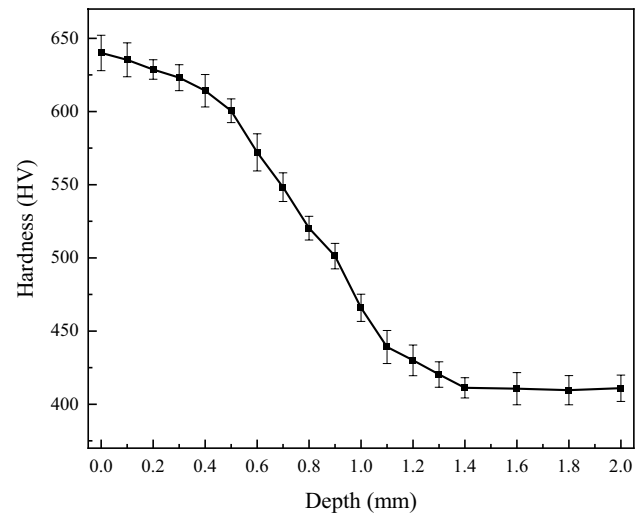
Table 1 18CrNiMo7-6 alloy steel element composition (wt%)

Element	C	Cr	Ni	Mn	Si	Mo	P	S	Fe
Content	0.21	1.58	1.4	0.72	0.34	0.26	0.01	0.004	Rest

**Fig. 1** Carburising heat treatment process

potential 1.1% for diffusion. The material was cooled to 830 °C, held for 60 min at 0.9% carbon potential, and then quenched to room temperature in oil, and finally heated to 180 °C for 3 h tempering. Figure 1 shows a diagram of the carburising heat treatment process.

After carburising and quenching, the material element composition changed, the material surface carbon content increased, and its surface has high hardness and anti-fatigue performance. According to the relevant research [28], scanning electron microscopy (SEM) was used to observe the metallographic structure of carburising heat treatment 18CrNiMo7-6 steel and electron back-scattered diffraction (EBSD) was applied to quantitatively analyse the phase content. The results showed that the metallographic structure of the carburised layer mainly retained austenite and martensite. With the increase of the depth of the carburised layer, the content of retained austenite decreased, the content of martensite increased, and the microstructure of martensite changed from flake to lath. The hardness distribution of the carburised 18CrNiMo7-6 steel surface modification layer was measured. Wire-cutting technology was used to cut a small part of the sample along the cross-section direction, and then the cross-section was ground and polished. A Vickers hardness tester was used to measure the hardness distribution of the sample perpendicular to the surface and along the depth direction. The measurement results are presented in Fig. 2. According to relevant standard documents [29], the depth of the carburised layer is the vertical distance from the sample surface to the Vickers hardness value of 550 HV. Figure 2 shows that the hardness reaches the maximum value of 640 HV on the surface of the carburised layer and decreases gradually along the depth direction. The hardness

**Fig. 2** Hardness distribution of surface modification layer of carburised heat treatment sample

value at 0.7 mm from the surface of the sample is 548.3 HV and finally stabilises at 410 HV of the base material. Therefore, the depth of the carburised layer of the sample is 0.7 mm.

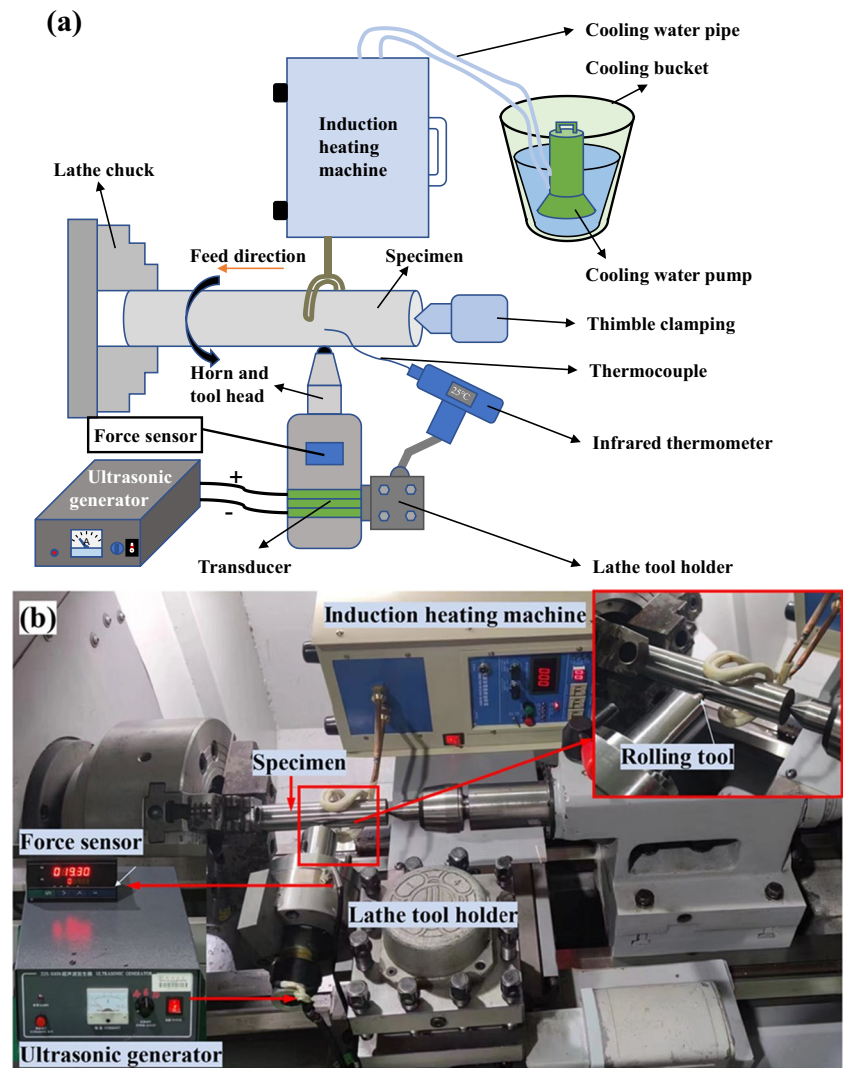
The carburised 18CrNiMo7-6 steel sample used in this study is a cylindrical sample of diameter 35 mm with length of 150 mm. Before the USRP experiment, the sample has to be ground on the MKA1320/H grinding machine to remove the black oxide skin on the surface.

2.2 Experimental equipment

The IH-USRP experiment was executed on the CAK4085 numerical control lathe. The entire experimental equipment consisted of two parts: USRP equipment and induction heating equipment. Figure 3 shows the schematic of the experimental equipment.

The USRP equipment is composed of an ultrasonic generator, a transducer, a horn, and a rolling tool head. The ultrasonic generator converts low-frequency current into high-frequency energy and supplies it to the transducer. Thereafter, the transducer converts the energy into ultrasonic vibrations, and the tiny vibration is amplified and transmitted to the rolling tool head through the horn. The rolling tool head contains the rolling ball, and the rolling ball uses silicon nitride ceramic material to reduce the conduction of the temperature from the sample surface to the USRP equipment during the IH-USRP as much as possible.

Fig. 3 IH-USRP device: **a** schematic and **b** photo of experimental device



This material not only insulates the heat, but also has high temperature resistance, high hardness, and light weight. The rolling ball selects three small balls of ϕ 4 mm to support a large ball of ϕ 8.731 mm to reduce the friction of the rolling ball inside the rolling tool head. The inner hole of the rolling tool head is designed to accommodate the rolling ball suitable. In addition, a force sensor is installed inside the USRP device, and the force sensor adopts a strain gauge sensor with high-precision wheel-spoke structure, with a measuring range of 0–100 kg. It has the advantages of strong anti-bias load ability, high precision, good sealing, and stable and reliable performance. The induction area of the force sensor is clamped on the horn through two flanges, and the exterior of the force sensor is fixed with the shell of the USRP device by bolting. When the rolling tool head is subjected to force, the pressure is transferred to the induction area of the force sensor through the rolling tool head and the horn. Then, the strain gauge in the force sensor generates an electrical signal

to be transmitted to the external digital display meter. Thus, the pressure value can be read out.

The induction heating equipment consists of high-frequency induction heating machine, induction heating coil, cooling water pump, and cooling bucket. The model of high-frequency induction heating machine is TGG-15 kw. The induction heating coil is wound by a round copper tube and the shape is an open U-shaped coil. The gap between the coil and the sample is 5–15 mm, which can ensure that the sample and induction heating coil can be fully coupled and provide maximum heating efficiency. The high-frequency induction heating machine is placed on the slide box of the CNC lathe and moves synchronously with the USRP equipment. In the process of induction heating, the induction heating equipment needs to continuously circulate cooling water through the cooling water pump and cooling water bucket to prevent the machine from overheating. In addition, to measure the induction heating process temperatures of

the sample, an infrared thermometer with a thermocouple is also used.

2.3 Measuring equipment and method

During the IH-USRP, the sample temperature is measured by an infrared thermometer installed with a thermocouple, which directly contacts the measuring position of the workpiece. After the IH-USRP experiment is completed, the sample is tested to detect the residual stress and microhardness and surface roughness.

Residual stress has a significant influence on the properties of the mechanical parts, and high residual compressive stress can effectively restrain the crack initiation [30]. The residual stress is measured by an X-ray residual stress analyser. The device uses Bragg's law to calculate the residual stress by measuring the rotation angle and azimuth angle of the X-ray entering the grain boundary of the material. By using electro-dissection layer equipment, we measure the residual stress distribution along the depth direction. The electrochemical corrosion method is used to layer the sample. The corrosion solution is saturated NaCl solution, the voltage used is 20 V, the layering time is 5 s, and the layering depth is 10 μm . The microhardness is measured by a HVW-1000Z Vickers automatic microhardness tester. The selected loading speed is 0.05 mm/s, the loading time is 10 s, and the load is 5 N. Surface roughness and surface topography are important indexes to evaluate the USRP sample surface quality. The sample is tested by NPFLEX 3D surface topography measuring equipment. The surface roughness of samples are evaluated by the arithmetical mean deviation of profile Ra and the maximum profile height of profile Rz. To accurately evaluate the residual stress, hardness, and surface roughness, and to ensure data reliability, each USRP parameter processing area takes three points to measure and find the average value. In addition, the metallographic structure of the sample can be observed by VHX-2000E optical microscope (OM), which can magnify the sample by 20–5000 times. Before observing the metallographic structure of the sample, the wire cutting technique should be used to cut the observed part into a small sample approximately $10 \times 10 \times 5$ mm, and the testing surface should be ground, polished, and corroded.

3 Results and analysis

3.1 Temperature gradient of sample in induction heating process

Induction heating has a skin effect, and the induced current in the workpiece is AC current, which is mostly distributed on the sample surface and decreases exponentially from the surface to the inner layer. For cylindrical workpieces, if the

surface current is I_0 , then the current density along the workpiece radius x direction can be expressed as follows [31]:

$$I_x = I_0 e^{-\frac{x}{\delta}} \quad (1)$$

where δ is the depth of current penetration, which can also be called heating layer depth.

In the process of induction heating, the energy of the metal being heated is first generated in the δ layer, and the inner metal is heated by heat conduction. At the distance of $(2.5 - 3)\delta$ from the surface of the workpiece, the current density almost drops to zero. The current depth can be received according to Eq. (2) [32]:

$$\delta = 5030 \sqrt{\frac{\rho}{f\mu}} (\text{cm}) \quad (2)$$

where ρ is the resistivity of the workpiece ($\Omega \text{ cm}$), μ is the relative permeability, and f is the power frequency.

In general, as the temperature rises, the metal resistivity increases, and the relative permeability decreases. In this experiment, the temperature does not change much, so the temperature effect on the resistivity and relative permeability of the workpiece is ignored. At the temperature of 100 $^\circ\text{C}$, for carburised 18CrNiMo7-6 steel, the resistivity is approximately $0.25 \times 10^{-4} \Omega \cdot \text{cm}$, the relative permeability is around 195 [31], and the frequency of induction heating power is 30 kHz. Thus, we can calculate the current penetration depth $\delta = 0.104\text{mm}$. According to this result, at the beginning of heating, the heating occurs on the surface, and then gradually conducts to the interior, and the heating layer thickness increases with the extension of time.

The temperature of the eddy current penetration layer within a certain time and the development speed of the heating layer to the interior depends on the energy provided to the unit surface area of the part in per-unit time, that is, the specific power P_0 . This parameter can be adjusted by adjusting the heating power knob on the high-frequency induction heating machine.

To better control the sample heating temperature during the IH-USRP experiment and reduce the error caused by the heating temperature deviation on the experiment results, the variation of the sample temperature with time and the gradient distribution along the diameter direction are measured when the heating power is 430 W. When measuring, a thermocouple probe is used to touch the side of the heated workpiece, take a measurement at every 2-mm depth, and measure three times to find the average value. The result is shown in Fig. 4.

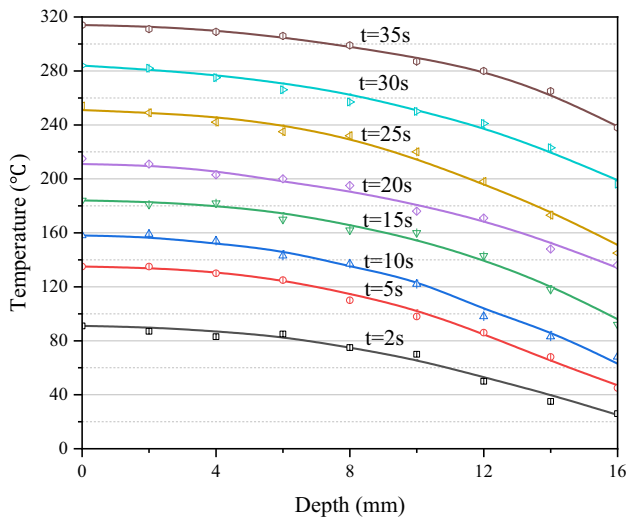


Fig. 4 Temperature gradient distribution of the sample during the induction heating process

3.2 Determination of process parameters for IH-USRP experiment

3.2.1 USRP at room temperature

To explore reasonable process parameters of the IH-USRP experiment, the USRP was executed at room temperature, the effect of various USRP parameters on the surface modification layer of carburised 18CrNiMo7-6 steel sample was investigated through single-factor experiment. Taking the residual stress as the evaluation standard, we studied the effects of different static pressures, rotation speeds, feed rates, amplitudes, and number of passes. Five different levels are set for each factor. For the amplitude used in the USRP experiment, we use an ultrasonic amplitude measuring instrument (model YP0901B) to determine the amplitude of vibration. The instrument, a special equipment for measuring ultrasonic amplitude, has a measuring range of 1–1200 μm , measuring accuracy of 2 μm , and measurable ultrasonic frequency range of 50 Hz–100 MHz, and can rotate at any angle. When measuring, we align the ultrasonic amplitude

measuring instrument with the rolling tool head and start the ultrasonic rolling equipment. The reading displayed by the ultrasonic amplitude measuring instrument is the amplitude in the current state. The ultrasonic generator we used has three blocks of low, middle, and high. The amplitudes of the three different blocks measured by our research group are 4, 6, and 10 μm . Therefore, the amplitudes of the three known values can be obtained by directly adjusting the three different gears in the follow-up experiments, thereby greatly simplifying the operation steps. However, because of the limitations of the ultrasonic generator, we can only use these three amplitudes for subsequent experiments. The designed experimental scheme is listed in Table 2.

After USRP at room temperature is completed, the residual stress of the USRP sample surface is measured. Figure 5 shows the measurement results. We can observe that the residual compressive stress is introduced into the sample surface after USRP. With the increase of static pressure, rotation speed, feed rate, and number of passes, the residual compressive stress first increases and then decreases. It continues to increase as the amplitude increases. The residual compressive stress of the sample surface reaches the maximum when static pressure is 500 N, rotation speed is 50 r/min, feed rate is 0.08 mm/r, amplitude is 10 μm , and number of passes is 2. However, under the amplitude of 10 μm , the operation of the USRP equipment is unstable. When the static pressure is greater than 400 N, the larger force has a negative impact on the thimble clamping of the lathe, so the 6 μm amplitude and 400 N static pressure are selected as the process parameters for the subsequent IH-USRP experiment. The other parameters are 50 r/min rotation speed, 0.08 mm/r feed rate, and 2 passes.

3.2.2 Determination of heating temperature

During the IH-USRP experiment, to guarantee that the heating temperature will not destroy the previous heat treatment state of the sample, the heating temperature should be lower than the martensitic transformation temperature, which is related to the sample carbon content and can be calculated according to Eq. (3) [22]. After

Table 2 Single-factor experimental scheme of USRP at room temperature

No	Static pressure (N)	Rotation speed (r/min)	Feed rate (mm/r)	Vibration Amplitude (μm)	Number of passes	Prediction items
1	200/300/400/ 500/600	100	0.08	6	2	Residual stress
2	400	25/50/75/100/125	0.08	6	2	
3	400	100	0.04/0.08/0.12/0.16/0.20	6	2	
4	400	100	0.08	4/6/10	2	
5	400	100	0.08	6	1/2/3/4/5	

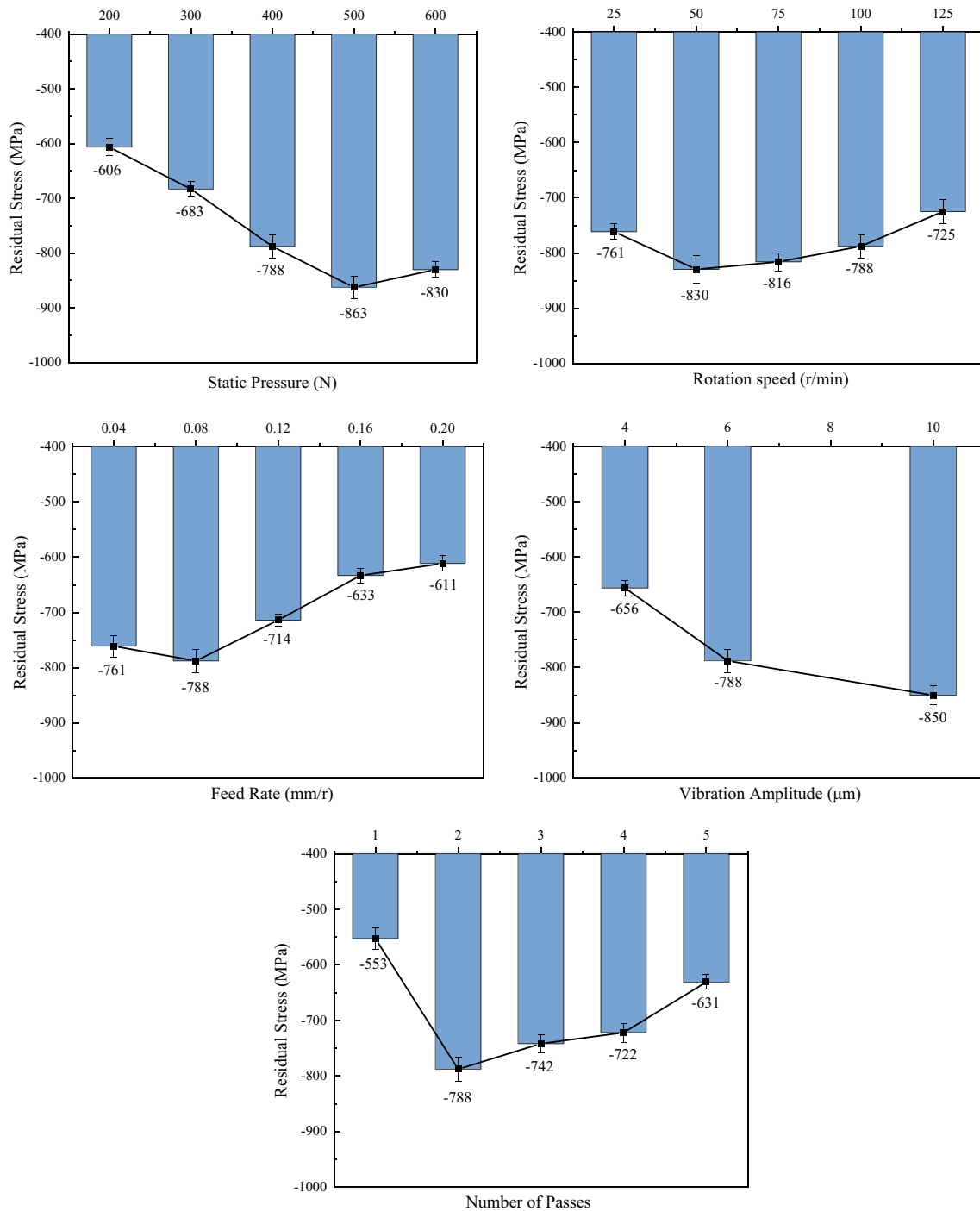


Fig. 5 Effect of USRP parameters on residual stress of sample surface at room temperature

carburising heat treatment, the highest sample carbon content at approximately 0.8% [33] is on the surface layer, and the carbon content gradually decreases as it gets closer to the centre. Based on the surface layer carbon content, the lowest martensitic transformation temperature of carburised 18CrNiMo7-6 steel is calculated as 264 °C.

$$M_s = 520 - [\%C] \times 320 \tag{3}$$

To verify this conclusion, Fig. 6 shows the metallographic diagrams of the surface microstructure of the samples heated to 250 °C and 300 °C observed on the OM. The martensite structure of the sample heated at 250 °C

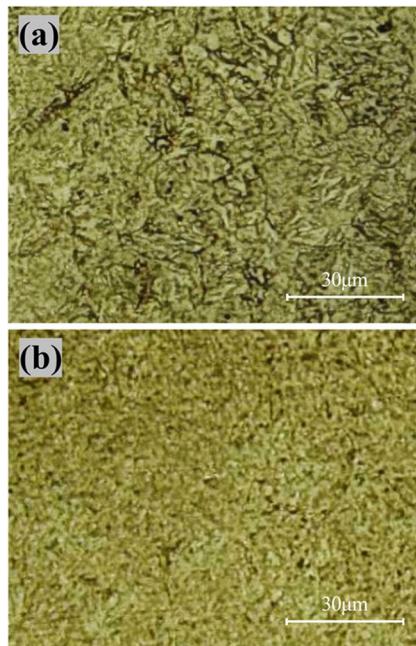


Fig. 6 Metallographic diagram at various temperatures: **a** 250 °C and **b** 300 °C

is visible on the diagram, but when heated to 300 °C, the clear martensite boundary becomes blurred and the martensite lath fuses, indicating that the martensite structure has changed. Therefore, the heating temperatures selected in the IH-USRP experiment are 100, 150, 200, and 250 °C. Moreover, two control groups were added to the experiment: one was USRP at 25 °C and the other was USRP at 300 °C.

According to the preceding conclusions and the lathe and USRP equipment actual working conditions, the IH-USRP experimental scheme is established and listed in Table 3. The experimental parameters of the IH-USRP are 400 N static pressure, 50 r/min rotation speed, 0.08 mm/r feed rate, 6 μm amplitude, and 2 passes. Taking temperature as a single-factor variable, the surface integrity of carburised 18CrNiMo7-6 steel after USRP at various temperatures is studied. The sample are rolled into two sections at each temperature to guarantee data reliability, and the rolling length of each section is 10 mm. Figure 7 shows the samples processed by USRP at various temperatures.

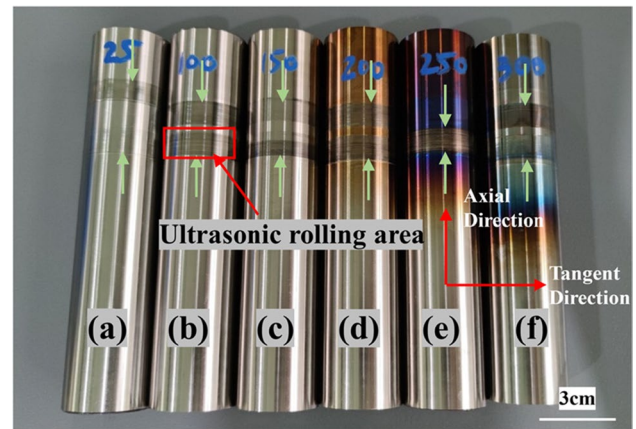


Fig. 7 USRP samples at various temperatures: **(a)** USRP at 25 °C, **(b)** USRP at 100 °C, **(c)** USRP at 150 °C, **(d)** USRP at 200 °C, **(e)** USRP at 250 °C, and **(f)** USRP at 300 °C

3.3 Residual stress

Figures 8 and 9 show the surface residual stress and residual stress distribution along the depth of the USRP samples at various temperatures. Figure 8 shows that the original sample has been ground, the initial axial residual stress on the surface is residual compressive stress, and the magnitude is -469 MPa. The tangential residual stress is residual tensile stress and the magnitude is 113 MPa. After IH-USRP, the axial and tangential residual stresses are both residual compressive stresses, and are obviously improved. They both increase at first and then decrease as the heating temperature increases, but the tangential residual stress is smaller. The axial and tangential residual stresses of USRP reach the maximum at 250 °C. To facilitate the analysis, the subsequent measurement only measures the axial residual stress.

Figure 9 shows that with the heating temperature increases from 25 to 250 °C, the residual compressive stress on the sample surface increases by 29% from -843 to -1088 MPa, the maximum residual compressive stress increases by 25.5% from -1013.03 to -1271.46 MPa. The depth of residual compressive stress increases from 1700 to 2450 μm and the depth of maximum residual compressive stress increases from 200 to 400 μm. The parameters show that the heating temperature is beneficial to the introduction of residual compressive stress after USRP. In the case of heating, the yield strength of the material decreases, making it easier to

Table 3 Experimental parameters of IH-USRP

Frequency (kHz)	Temperature (°C)	Static pressure (N)	Rotation speed (r/min)	Feed rate (mm/r)	Vibration Amplitude (μm)	Number of passes
28	25/100/150/ 200/250/300	400	50	0.08	6	2

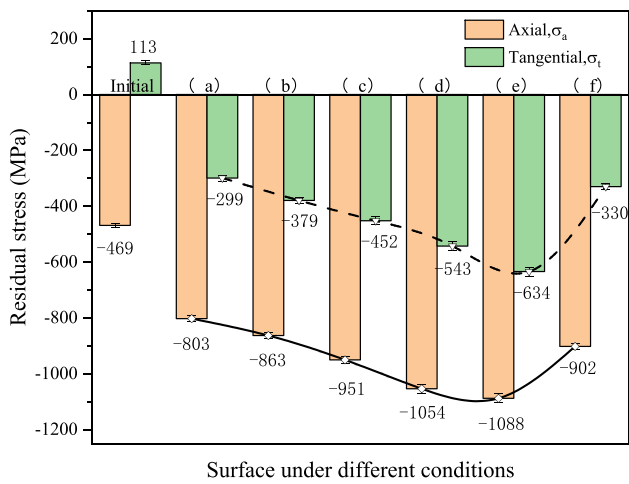


Fig. 8 Surface residual stress of USRP samples at various temperatures: (a) USRP at 25 °C, (b) USRP at 100 °C, (c) USRP at 150 °C, (d) USRP at 200 °C, (e) USRP at 250 °C, and (f) USRP at 300 °C

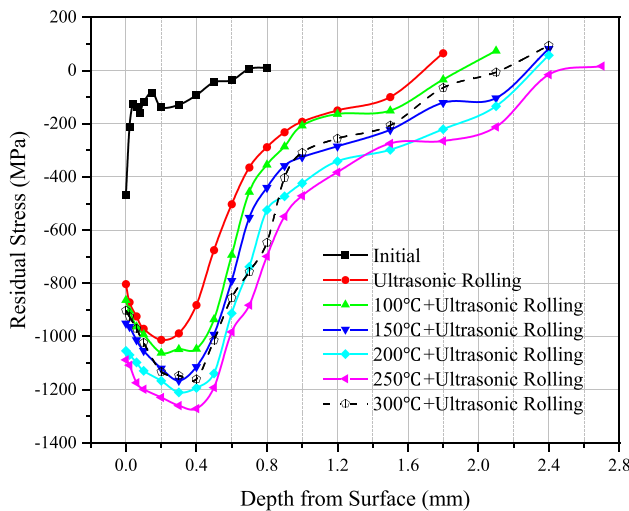


Fig. 9 Residual stress distribution along the depth of USRP samples at various temperatures

undergo deformation strengthening, thereby increasing the depth of the residual compressive stress layer [22]. Larger residual compressive stress and residual compressive stress depth can restrain the surface crack initiation and increase the anti-fatigue performance of the material. The results show that IH-USRP at the appropriate temperature plays a positive role in enhancing the sample anti-fatigue performance. However, when the heating temperature exceeds the martensitic transformation temperature to 300 °C, the residual compressive stress and the depth of the maximum residual compressive stress decrease. Although a higher heating temperature is conducive to greater plastic deformation of the material, the microstructure of the material

undergoes dynamic recrystallisation because of the influence of temperature, resulting in a decrease in the residual compressive stress [21]. When the temperature is extremely high, the material undergoes a serious overaging effect and a high rate of static/dynamic recovery [19], which is also a reason for the decrease in residual compressive stress.

3.4 Microhardness

Figure 10 shows the changing trend of surface hardness of USRP samples at various temperatures. The measurement results show that the sample surface hardness is 640 HV before USRP. After USRP at room temperature, the surface hardness greatly improves to 858.5 HV. However, the surface hardness does not improve visibly after IH-USRP, and even decreases slightly at 300 °C. As the heating temperature increases, the surface hardness increases at first and then decreases. The highest surface hardness is obtained by USRP at 250 °C, but is still lower than that of the USRP sample at room temperature. Figure 11 shows the hardness distribution of USRP samples with depth at various temperatures. The hardness of samples with or without USRP both decreases gradually from the surface to the core, and finally tends to the hardness of the matrix material 410 HV. However, USRP has a certain effect on the surface layer, which increases the hardness of the surface layer, and the most obvious improvement in the hardness is USRP at room temperature. With the rise of the heating temperature, the influence layer of USRP on the sample hardness deepens gradually. The hardness influence layer of the USRP sample is 1.5 mm at room temperature. When the sample is heated to 250 °C, the hardness influence layer increases to

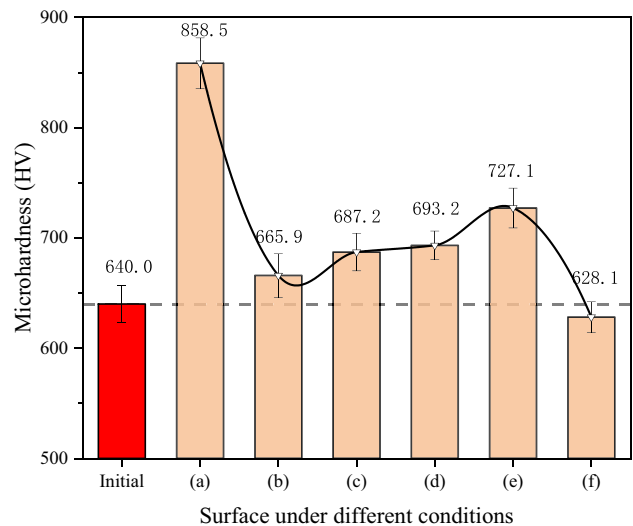


Fig. 10 Surface hardness of USRP samples at various temperatures: (a) USRP at 25 °C, (b) USRP at 100 °C, (c) USRP at 150 °C, (d) USRP at 200 °C, (e) USRP at 250 °C, and (f) USRP at 300 °C

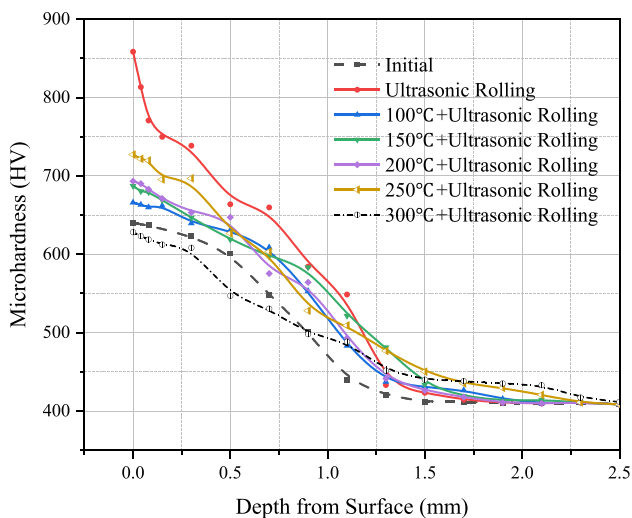


Fig. 11 Hardness distribution with depth of samples at various USRP temperatures

1.8 mm. When heated to 300 °C, although the influence layer of USRP on the hardness is further deepened, it has an adverse effect on the surface hardness, and the surface layer hardness at 0–700 μm is even lower than that of the sample without USRP.

Analysing the above results, we obtain the following conclusions. During USRP, the material surface produces plastic deformation and strain hardening effect, so the surface hardness is effectively improved after USRP. When the sample is subjected to USRP at a certain heating temperature, because of the influence of temperature, the lack of cold work hardening on the surface of the sample leads to a decrease in the hardness of the material surface compared with USRP at room temperature, which was the same result reported in another paper [17]. In addition, when USRP is carried out at room temperature, lubricating oil is added to the contact surface, and good lubrication helps increase the USRP surface strengthening effect and improve the surface hardness obviously. However, because of the high temperature in IH-USRP, the contact surface cannot be lubricated effectively, which leads to a decline of the USRP effect and subsequently affects the sample surface hardness after USRP [17]. The change of the surface hardness of the sample when the temperature is in the range of 100–250 °C deserves in-depth analysis. In this range, as the heating temperature increases, the surface hardness of the sample also increases, indicating that heating has a beneficial effect. The increase of heating temperature reduces the surface strain energy of the material, which is beneficial to produce larger plastic deformation on the surface of the sample and a deeper work hardening layer [34]. The large plastic deformation is conducive to grain refinement, and the finer the grain, the higher the surface hardness of the material [35]. In addition, the

sample is not easy to cool after IH-USRP at a higher temperature. During this process, carbides are precipitated on the surface of the sample due to the effect of temperature, which also increases the surface hardness of the sample [18]. However, when the heating temperature is extremely high, such as USRP at 300 °C, the microstructure of the sample material changes, which has an adverse effect, so the surface hardness becomes lower than the original sample.

3.5 Surface roughness and surface topography

USRP causes large plastic deformation on the surface of the material through direct contact between the rolling ball and the surface, thereby affecting the surface roughness of the material. During USRP, the magnitude of rolling pressure and number of passes affects the surface roughness of the sample, and then the fatigue life of the material [36]. Celik [37] studied the effects of different static pressures, feed rates, and number of passes on the surface roughness of Inconel718 alloy and found that the suitable process parameters could significantly reduce the surface roughness of the sample, and the number of passes have the greatest influence on the surface roughness, followed by feed rate and static pressure. Figure 12 shows the 3D topography of the USRP samples at various temperatures. After USRP, the sample surface undergoes plastic deformation, which makes the surface smoother under the rolling pressure. This condition is beneficial to improve the material surface quality and reduce the stress concentration [38].

Figure 13 shows the variation curve of surface roughness R_a of the USRP samples at various temperatures. The measured values of R_z are listed in Fig. 13 at the same time and the change trends are roughly the same. The initial surface roughness before USRP is measured at R_a 0.194 μm and R_z 2.421 μm . After USRP, compared with the initial sample, the surface roughness has an obvious decrease, which indicates that USRP has a better finishing effect. The surface roughness after USRP at 100 °C is the lowest, which is obviously lower than USRP at room temperature. When the heating temperature is 100, 150, 200, 250, and 300 °C, compared with the initial surface roughness, the surface roughness R_a after IH-USRP decreases by 59.8%, 48.5%, 34.5%, 15.5%, and 12.3%, respectively. These results show that under the same USRP parameters, the appropriate heating temperature is beneficial to the softening of the material and can effectively improve the degree of plastic deformation, which enables the material to obtain a better surface modification layer so that its microstructure and mechanical properties are further improved [3]. However, the surface roughness of USRP at 250 °C and 300 °C is slightly higher than that of the samples with USRP at room temperature. The surface roughness levels of the sample after USRP at 300 °C are R_a 0.194 μm and R_z 0.441 μm , which are higher than those of the

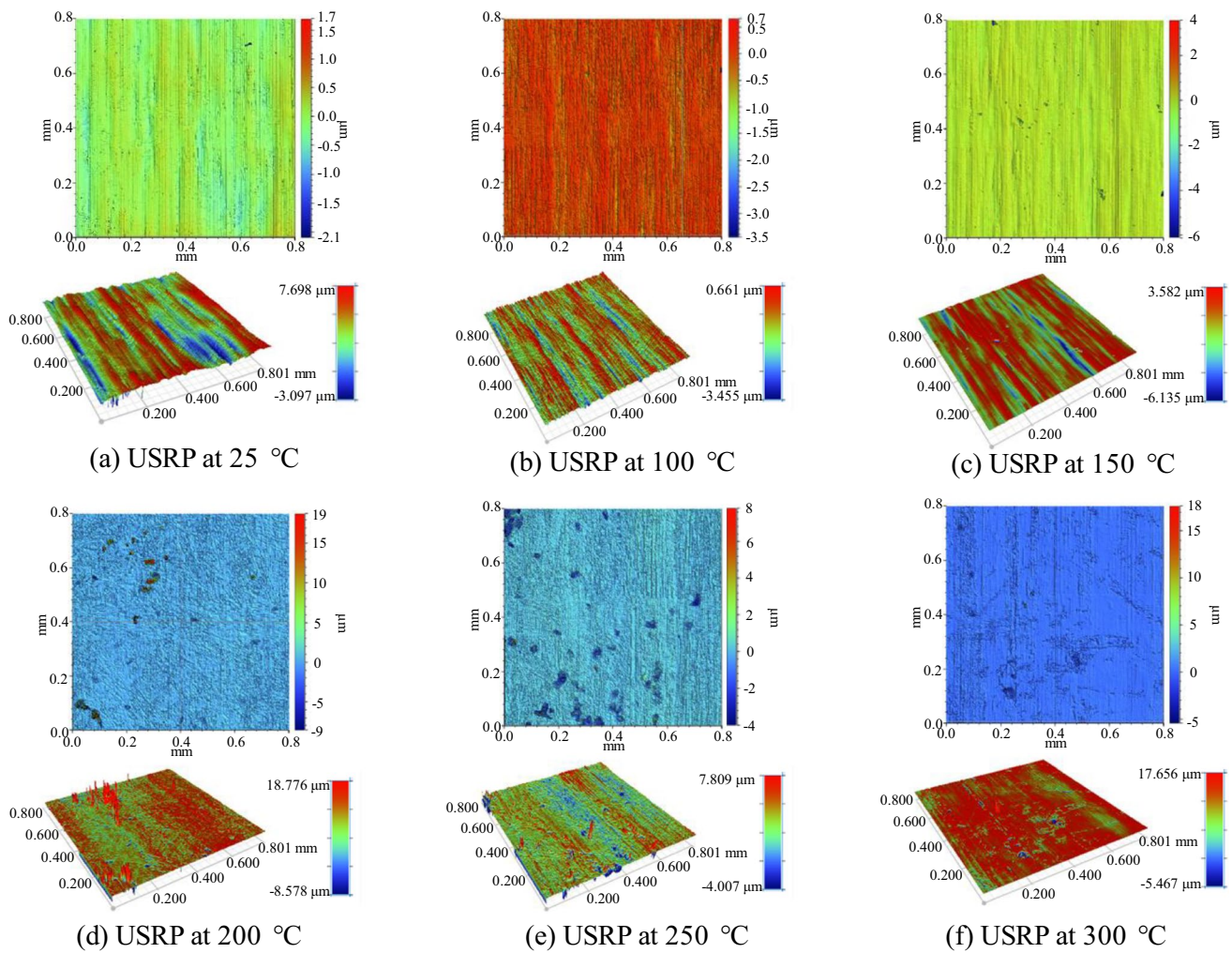


Fig. 12 Surface topography of USRP samples at various temperatures

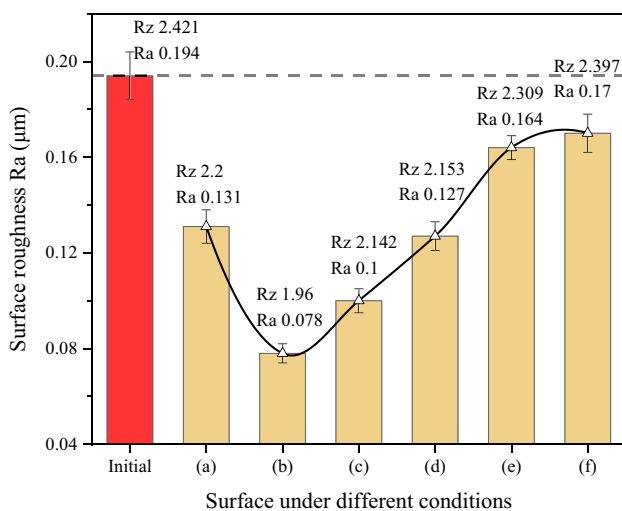


Fig. 13 Surface roughness of USRP samples at various temperatures: (a) USRP at 25 °C, (b) USRP at 100 °C, (c) USRP at 150 °C, (d) USRP at 200 °C, (e) USRP at 250 °C, and (f) USRP at 300 °C

sample of USRP at room temperature, but still lower than the initial sample. The reason is that surface roughness increase is due to the material surface dry friction behaviour and the higher heating temperature. During IH-USRP, a slight bond occurs between the heated material and the rolling ball [17], which is also evident from the surface topography of the USRP samples at various temperatures. As the heating temperature increases, the sample surface is oxidised, which is another reason for the increase in the surface roughness of the sample [22].

4 Optimisation of IH-USRP parameters based on grey relational analysis

4.1 Orthogonal experiment

Residual stress, microhardness, and surface roughness are three important indexes that affect the anti-fatigue

properties of materials. To obtain the best anti-fatigue properties, we expect the surface residual compressive stress and the hardness to be the largest and the surface roughness to be the smallest. Celik [37] used a similar method to study the effects of four different static pressures, feed rates, and number of passes on the surface roughness of Inconel 718 alloys, and obtained the optimal process parameters for achieving the best surface roughness and the order of significance of the effect on surface roughness. Therefore, based on previous work, static pressure, feed rate, rotation speed, and temperature are selected as processing factors, while the amplitude remains at 6 μm and the number of passes are 2. Four levels were selected for each factor and the orthogonal experiment was designed. During the study, a blank factor X was added to form $L_{16}(4^5)$. The range of designed experimental parameters is listed in Table 4. The residual stress, microhardness, and surface roughness are used as evaluation indexes to optimise the parameters. Table 5 shows the orthogonal

Table 4 $L_{16}(4^5)$ orthogonal experimental table

Level	Factors					X
	Static pressure (N)	Feed rate (mm/r)	Rotation speed (r/min)	Temperature ($^{\circ}\text{C}$)		
1	100	0.04	30	25	/	/
2	200	0.08	50	100	/	/
3	300	0.12	100	200	/	/
4	400	0.16	200	250	/	/

Table 5 $L_{16}(4^5)$ orthogonal experimental results

No	Factors					X	Experimental results		
	Static pressure (N)	Feed rate (mm/r)	Rotation speed (r/min)	Temperature ($^{\circ}\text{C}$)	Surface roughness (μm)		Surface hardness (HV)	Residual stress (MPa)	
1	100	0.04	30	25	/	0.073	691.71	769.85	
2	100	0.08	50	100	/	0.081	671.3	774.73	
3	100	0.12	100	200	/	0.107	676.31	921.74	
4	100	0.16	200	250	/	0.168	691.68	896.4	
5	200	0.04	50	200	/	0.117	683.95	976.35	
6	200	0.08	30	250	/	0.157	723.56	987.64	
7	200	0.12	200	25	/	0.125	699.34	763.94	
8	200	0.16	100	100	/	0.092	663.1	786.92	
9	300	0.04	100	250	/	0.154	709.73	1049.32	
10	300	0.08	200	200	/	0.143	669.24	985.7	
11	300	0.12	30	100	/	0.078	669.53	828.46	
12	300	0.16	50	25	/	0.088	691.68	793.47	
13	400	0.04	200	100	/	0.081	673.95	857.74	
14	400	0.08	100	25	/	0.12	758.48	787.94	
15	400	0.12	50	250	/	0.143	729.35	1059.21	
16	400	0.16	30	200	/	0.126	674.68	1007.25	

experimental results. For convenience of analysis, the surface residual stress takes its absolute value.

4.2 Analysis of grey relational degree

According to the experimental results listed in Table 5, the processing parameters are optimised by multi-objective optimisation. Firstly, the data are normalised. We hope that the index of surface hardness and residual stress can be as large as possible. This index is calculated in Eq. (4) as follows [39]:

$$x_{ij} = \frac{y_{ij} - \min_j y_{ij}}{\max_j y_{ij} - \min_j y_{ij}} \quad (4)$$

where $\max_j y_{ij}$ is the maximum value in the j column of the data column and $\min_j y_{ij}$ is the minimum value in the j column of the data column.

We also hope that the index of surface roughness can be as low as possible. It is calculated in Eq. (5) as follows:

$$x_{ij} = \frac{\max_j y_{ij} - y_{ij}}{\max_j y_{ij} - \min_j y_{ij}} \quad (5)$$

The degree of correlation between the normalised data and the ideal value can be expressed by grey correlation coefficient as

$$\xi_{ij} = \frac{\min_i \min_j |x_i^0 - x_{ij}| + \zeta \max_i \max_j |x_i^0 - x_{ij}|}{|x_i^0 - x_{ij}| + \zeta \max_i \max_j |x_i^0 - x_{ij}|} \quad (6)$$

where x_i^0 is the ideal value of the experimental data, which is 1, and ζ is the resolution coefficient with a value in the range of [0,1]. The resolution coefficient ζ can be obtained as follows:

$$\Delta_v = \frac{1}{nm} \sum_{i=1}^m \sum_{j=1}^n |x_i^0(j) - x_{ij}| \quad (7)$$

$$\varepsilon_{\Delta} = \frac{\Delta_v}{\Delta_{max}} \quad (8)$$

$$\Delta_{max} \leq 2\Delta_v \quad (9)$$

$$\varepsilon_{\Delta} < \zeta < 1.5\varepsilon_{\Delta} \quad (10)$$

From the calculation of the preceding formulas, we can obtain $\Delta_v = 0.57$, $\varepsilon_{\Delta} = 0.57$. Due to $\varepsilon_{\Delta} < \zeta < 1.5\varepsilon_{\Delta}$, that is $0.57 < \zeta < 0.86$, we take $\zeta = 0.6$. Finally, through the calculation of the grey correlation degree, multiple objectives are transformed into the evaluation of a single target, as shown in Eq. (11), and the value of the grey correlation degree is shown in Table 6.

$$\gamma_{ij} = \frac{1}{k} \sum_{i=1}^k W_k \xi_{ij} \quad (11)$$

where γ_{ij} is the grey correlation degree value, W_k is the weight index in the experimental results, and the weight index has a value of 1.

According to the calculation results in Table 6, the mean value of the grey correlation degree of each control factor of IH-USRP can be calculated and listed in Table 7.

Delta in Table 7 is the difference between the maximum and minimum grey correlation degrees of each factor. The order of significance of four control factors on the surface integrity influence can be judged by the value. The higher the value, the more significant is the influence. Table 7 is shown in graphic form as Fig. 14. The larger the grey correlation degree mean value is, the better the corresponding performance characteristics are. Thus, when the grey correlation degree mean value reaches the maximum, the corresponding processing parameters are the optimal process parameters. Figure 14 shows that the optimised process parameters are as follows: 400 N static pressure, 0.04 mm/r feed rate, 50 r/min rotation speed, and 250 °C heating temperature. According to the research results in Section 3, although USRP at 100 °C for the surface roughness index is the best, it is only obtained by single factor analysis of surface roughness. The surface integrity index is analysed

Table 6 Calculation results of grey correlation degree

No	Grey correlation coefficient			Grey relational degree
	Surface roughness (µm)	Surface hardness (HV)	Residual stress (MPa)	Calculated value
1	1.00	0.46	0.38	0.61
2	0.88	0.40	0.38	0.55
3	0.63	0.41	0.56	0.53
4	0.38	0.46	0.52	0.45
5	0.56	0.43	0.68	0.56
6	0.40	0.62	0.71	0.58
7	0.52	0.49	0.38	0.46
8	0.75	0.38	0.39	0.51
9	0.41	0.54	0.95	0.63
10	0.45	0.39	0.71	0.52
11	0.92	0.39	0.43	0.58
12	0.79	0.46	0.40	0.55
13	0.88	0.40	0.47	0.58
14	0.55	1.00	0.40	0.65
15	0.45	0.66	1.00	0.70
16	0.52	0.41	0.77	0.57

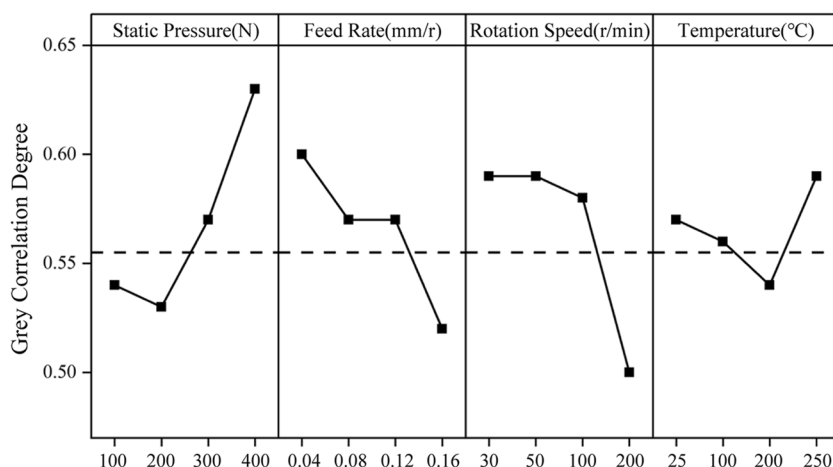
Table 7 Mean value of grey correlation degree

Level	Static pressure	Feed rate	Rotation speed	Temperature
1	0.54	0.60	0.59	0.57
2	0.53	0.57	0.59	0.56
3	0.57	0.57	0.58	0.54
4	0.63	0.52	0.50	0.59
Delta	0.1	0.08	0.09	0.05
Ranking	1	3	2	4

by considering multiple objectives to achieve the relatively optimal effect by comprehensively considering surface roughness, surface hardness, and surface residual stress. For the residual stress index, USRP at 250 °C is the best and USRP at 250 °C is relatively good for the surface hardness index. Therefore, according to the conclusions obtained in this section, the best surface integrity can be obtained by USRP when the heating temperature is 250 °C. According to the ranking order in Table 7, the effect on the surface integrity has the following order of significance: static pressure > rotation speed > feed rate > heating temperature. Wang et al. [40] used the same method to optimise the USRP parameters; they considered the influence of amplitude and concluded that the order of influence on the surface integrity is static pressure > rotation speed > feed rate.

In conclusion, although the effect of heating temperature on the surface integrity of the sample was not significant, the heating temperature had a certain effect on the single surface

Fig. 14 Effect of processing parameters on grey correlation degree



integrity parameters, especially residual compressive stress and surface roughness. When USRP was at 250 °C, the maximum surface residual compressive stress and residual compressive stress depth were obtained. Compared with USRP at room temperature, the surface residual compressive stress increased by 29% and the residual compressive stress depth increased from 1700 to 2450 μm . When USRP was at 100 °C, the minimal surface roughness was obtained. Compared with USRP at room temperature, the surface roughness Ra decreased by 40.5%. These results showed the value of heating temperature on the surface properties of the sample after USRP. This research conclusion has a certain guiding significance for the anti-fatigue manufacturing of materials.

5 Conclusions

In this paper, a single-factor USRP experiment of carburised 18CrNiMo7-6 steel was carried out and the optimum process parameters of USRP at room temperature were obtained. The experimental parameters of IH-USRP were determined based on the actual working conditions of the lathe and USRP equipment. Then, under these process parameters, the temperature field was introduced by induction heating to conduct IH-USRP. The residual stress, microhardness, and surface roughness of the USRP samples at various temperatures were compared. The grey correlation analysis method was used to optimise the process parameters of IH-USRP. The optimised process parameters and their order of significance on the surface integrity were obtained. The following conclusions can be drawn:

1. After USRP, the residual compressive stress was introduced into the sample surface. As the heating temperature increased from 25 to 250 °C, the surface residual compressive stress and depth of residual compressive stress increased continuously. The surface residual compressive stress and maximum residual compressive stress of the sample increased by 29% and 25.5% respectively; the residual compressive stress depth increased from 1700 to 2450 μm ; and the maximum residual compressive stress depth increased from 200 to 400 μm . However, when the heating temperature was higher than the material martensitic transformation temperature to 300 °C, the residual compressive stress decreased, which had an adverse effect.
2. Compared with USRP at room temperature, IH-USRP did not have a better effect on the surface hardness, and minimal difference was observed in the surface hardness after USRP at various temperatures. Although the surface hardness was lower than that of the USRP samples at room temperature, it was still higher than those of the initial samples. As the heating temperature increased from 25 to 250 °C, the influence layer of the surface hardness increased from 1.5 to 1.8 mm. When the heating temperature was higher than the material martensitic transformation temperature to 300 °C, although the hardness influence layer was still increasing, the sample surface hardness decreased and the hardness at the surface layer of 0–700 μm was even lower than that of the sample without USRP.
3. IH-USRP could still obtain a good surface finishing effect and the surface roughness obtained by USRP at 100 °C was the best, indicating that the appropriate heating temperature was conducive to material softening and plastic deformation. The surface roughness increased with the increase of heating temperature. The surface roughness of USRP at 250 °C and 300 °C was higher than that of USRP at room temperature, which could be due to the high heating temperature resulting in the adhesion of the sample surface during USRP.
4. The IH-USRP process parameters were optimised by grey correlation analysis method. According to the best surface integrity as the evaluation index, the optimal

process parameters were as follows: 400 N static pressure, 0.04 mm/r feed rate, 50 r/min rotation speed, and 250 °C heating temperature. The effects on surface integrity had the following order of significance: static pressure > rotation speed > feed rate > heating temperature.

Acknowledgements The authors appreciate the experimental support by Henan Key Engineering Laboratory for Anti-fatigue Manufacturing Technology. The authors also want to express our deep gratitude to the National Natural Science Foundation of China (No. 52001281).

Author contribution All the authors have made important contributions to this study. Zhihua Liu was responsible for the conception and revision of the paper and experimental guidance; Lingshuo Zheng and Peng Tang were responsible for the experimental work and the manuscript of the paper; Shengwei Qin was responsible for the heat treatment of materials. All the authors discussed the manuscript, read and approved the final manuscript.

Funding This work was supported by the National Natural Science Foundation of China (No. 52001281).

Data availability The data obtained in this study are available from the corresponding author on reasonable request.

Declarations

Ethical approval The authors state that this paper is an original work, it has not been published in any journals, and this research does not involve any ethical issues of humans or animals.

Consent to participate All authors are aware and satisfied with the authorship order and correspondence of the paper.

Consent to publication All the authors have consented to publication and have been approved by the institutions to which this work belongs.

Conflict of interest The authors declare no competing interests.

References

- Wang SH, Zhou YS, Tang JY, Tang K, Li ZMQ (2022) Digital tooth contact analysis of face gear drives with an accurate measurement model of face gear tooth surface inspected by CMMs. *Mech Mach Theory* 167:1–20. <https://doi.org/10.1016/j.mechmachtheory.2021.104498>
- Teimouri R, Amini S, Bami AB (2018) Evaluation of optimized surface properties and residual stress in ultrasonic assisted ball burnishing of AA6061-T6. *Measurement* 116:129–139. <https://doi.org/10.1016/j.measurement.2017.11.001>
- Tao GY, Luo XS, Sun QY, Duan HT (2023) The state of the art of ultrasonic surface rolling technology and its combination technology. *Surf Technol* 52(02):122–134. <https://doi.org/10.16490/j.cnki.issn.1001-3660.2023.02.011>
- Zhao JY, Zhou WH, Tang JY, Jiang TT, Liu HM (2022) Analytical and experimental study on the surface generation mechanism in shot peening. *Arch Civ Mech Eng* 22(3). <https://doi.org/10.1007/s43452-022-00431-7>
- Liu HW, Zheng JX, Guo YL, Zhu LX (2020) Residual stresses in high-speed two-dimensional ultrasonic rolling 7050 aluminum alloy with thermal-mechanical coupling. *Int J Mech Sci* 186. <https://doi.org/10.1016/j.ijmecsci.2020.105824>
- Bucior M, Kluz R, Trzepieciniski T, Jurczak K, Kubit A, Ochal K (2022) The effect of shot peening on residual stress and surface roughness of AMS 5504 stainless steel joints welded using the TIG method. *Materials* 15(24):8835–8849. <https://doi.org/10.3390/ma15248835>
- Pan XL, Zhou LC, Wang CX, Yu K (2023) Microstructure and residual stress modulation of 7075 aluminum alloy for improving fatigue performance by laser shock peening. *Int J Mach Tools Manuf* 184:1–15. <https://doi.org/10.1016/j.ijmactools.2022.103979>
- Sarma J, Kumar R, Sahoo AK, Panda A (2020) Enhancement of material properties of titanium alloys through heat treatment process: a brief review. *Mater Today Proc* 23:561–564. <https://doi.org/10.1016/j.matpr.2019.05.409>
- Luo X, Tan QY, Mo N, Yin Y, Yang YQ, Zhuang W, Zhang MX (2019) Effect of deep surface rolling on microstructure and properties of AZ91 magnesium alloy. *T Nonferr Metal Soc* 29(7):1424–1429. [https://doi.org/10.1016/S1003-6326\(19\)65049-1](https://doi.org/10.1016/S1003-6326(19)65049-1)
- Liu ZH, Zhang TZ, Yang MJ, Dai QL, Zhang YX (2020) Performance analysis of surface modification layer of 18CrNiMo7–6 gear steel treated by ultrasonic rolling. *J Zhengzhou Univ Eng Sci* 41(02):44–49. <https://doi.org/10.13705/j.issn.1671-6833.2020.03.016>
- Meng C, Zhao YC, Zhang XY, Wang X, He Y, Zhang J (2022) Research and application of ultrasonic rolling surface strengthening technology. *Surf Technol* 51(08):179–202. <https://doi.org/10.16490/j.cnki.issn.1001-3660.2022.08.015>
- Liu ZH, Zhang CH, Zhao H, Vincent J, Wang D (2021) Theoretical analysis and performance prediction on modified surface layer caused by ultrasonic surface rolling. *Int J Adv Manuf Technol* 113:1307–1330. <https://doi.org/10.1007/s00170-021-06642-1>
- Wang PC, Pan YZ, Liu YJ, Fu XL, Li HX (2021) Research on surface properties of Ti-6Al-4V alloy by multi-ultrasonic rolling. *Proc Inst Mech Eng C J Mech Eng Sci* 235(21):5594–5602. <https://doi.org/10.1177/0954406220984194>
- Han MZ, Zhang HX, Yan ZF, Li KW, Wang WX (2022) Improving fatigue properties of 18CrNiMo7-6 steel by surface strengthening. *Mater Lett* 328:72–83. <https://doi.org/10.1016/j.matlet.2022.133200>
- Qin SW, Zhang B, Zhao HH, Zhang YF (2020) Effect of transformation plasticity coefficient on residual stress of 18CrNiMo7–6 carburizing steel. *Surf Technol* 49(12):138–143. <https://doi.org/10.16490/j.cnki.issn.1001-3660.2020.12.015>
- Wei HL, Liu GQ, Xiao X, Zhao HT, Ding H, Kang RM (2013) Characterization of hot deformation behavior of a new microalloyed C-Mn-Al high-strength steel. *Mater Sci Eng A* 564:140–146. <https://doi.org/10.1016/j.msea.2012.11.099>
- Li G, Qu SG, Xie MX, Li XQ (2017) Effect of ultrasonic surface rolling at low temperatures on surface layer microstructure and properties of HIP Ti-6Al-4V alloy. *Surf Coat Technol* 316:75–84. <https://doi.org/10.1016/j.surfcoat.2017.01.099>
- Zhang CS, Shen XH, Wang JT, Xu CH, He JQ, Bai XL (2021) Improving surface properties of Fe-based laser cladding coating deposited on a carbon steel by heat assisted ultrasonic burnishing. *J Mater Res Technol* 12:100–116. <https://doi.org/10.1016/j.jmrt.2021.02.076>
- Juijerm P, Altenberger I (2006) Effect of high-temperature deep rolling on cyclic deformation behavior of solution-heat-treated Al-Mg-Si-Cu alloy. *Scr Mater* 56(4):285–288. <https://doi.org/10.1016/j.scriptamat.2006.10.017>

20. Liu J, Suslov S, Ren ZC, Dong YL, Ye C (2019) Microstructure evolution in Ti64 subjected to laser-assisted ultrasonic nanocrystal surface modification. *Int J Mach Tools Manuf* 136:19–33. <https://doi.org/10.1016/j.ijmactools.2018.09.005>
21. Liu ZQ, Liu X, Liu RP, Xiao ZY, Sanderson J (2023) Improved rolling contact fatigue performance of selective electron beam melted Ti6Al4V with the as-built surface using induction-heating assisted ultrasonic surface rolling process. *Appl Surf Sci* 617:1–12. <https://doi.org/10.1016/j.apsusc.2022.155467>
22. Luan XS, Zhao WX, Liang ZQ, Xiao SH, Liang GX, Chen YF, Zou SK, Wang XB (2020) Experimental study on surface integrity of ultra-high-strength steel by ultrasonic hot rolling surface strengthening. *Surf Coat Technol* 392:1–9. <https://doi.org/10.1016/j.surfcoat.2020.125745>
23. Lucia O, Maussion P, Dede EJ, Burdion JM (2014) Induction heating technology and its applications: past developments, current technology, and future challenges. *IEEE Trans Ind Electron* 61(5):2509–2520. <https://doi.org/10.1109/TIE.2013.2281162>
24. Hu JJ (2017) Effect of surface ultrasonic rolling processing on surface integrity and fatigue properties of 60Si2CrVAT spring steel. Dissertation, Guizhou University
25. Mei GY, Zhang KH, Ding JF (2010) Study on the effect of ultrasonic surface rolling processing parameters on the surface roughness of Q345 hydraulic prop. *Adv Mat Res* 910(102):591–594. <https://doi.org/10.4028/www.scientific.net/AMR.102-104.591>
26. Sun YG, Dang YG (2008) Improvement on grey T's correlation degree. *Syst Eng Theory Pract* 04:135–139. [https://doi.org/10.12011/1000-6788\(2008\)4-135](https://doi.org/10.12011/1000-6788(2008)4-135)
27. Yang M (2022) Practical heat treatment technical manual. China Machine Press, Beijing
28. Wang G, Sang XG, Zhang Y, Zhao MH, Xu GT, Peng ZL (2023) Carburization-induced microstructure evolution and hardening mechanism of 18CrNiMo7-6 steel. *J Mater Res Technol* 25:1649–1661. <https://doi.org/10.1016/j.jmrt.2023.06.050>
29. China SA (2006) GB/T 9450–2005 Steels-Determination and verification of the depth of carburized and hardened cases. National public service platform for standards information. <https://std.samr.gov.cn/>. Accessed 1 Jan 2006
30. Kanchanomai C, Limtrakarn W (2008) Effect of residual stress on fatigue failure of carbonitrided Low-Carbon steel. *J Mater Eng Perform* 17(6):879–887. <https://doi.org/10.1007/s11665-008-9212-x>
31. Zhang YH (2009) Numerical simulation of temperature field for the induction heating of the metal forging preform based on ANSYS. *Ind Heat* 38(02):23–26. <https://doi.org/10.3969/j.issn.1002-1639.2009.02.007>
32. Xu XF, Liu XG, Zhao M (2008) Study on numerical simulation technology of billet induction heating. *New Technol New Process* 10:77–80. <https://doi.org/10.3969/j.issn.1003-5311.2008.10.028>
33. Qin SW, Zhang YF, Zhang B (2020) Study on diffusion coefficient of carburizing process simulation of 18CrNiMo7-6 steel. *J Zhengzhou Univ Eng Sci* 41(02):56–60. <https://doi.org/10.13705/j.issn.1671-6833.2020.03.006>
34. Hong SI (1985) Influence of dynamic strain aging on the apparent activation volume for deformation. *Mater Sci Eng* 76:77–81. [https://doi.org/10.1016/0025-5416\(85\)90082-5](https://doi.org/10.1016/0025-5416(85)90082-5)
35. Prakash NA, Gnanamoorthy R, Kamaraj M (2010) Microstructural evolution and mechanical properties of oil jet peened aluminium alloy, AA6063-T6. *Mater Des* 31(9):4006–4075. <https://doi.org/10.1016/j.matdes.2010.04.057>
36. Celik M, Caydas U, Akyuz M (2022) The influence of roller burnishing process parameters on surface quality and fatigue life of AA 7075-T6 alloy. *Materwiss Werkstsch* 53(5):608–616. <https://doi.org/10.1002/mawe.202100291>
37. Celik M (2023) Investigation of the effects of roller burnishing on the surface quality of Inconel 718 alloy. *Firat Univ Müh Bilim Derg* 35(1):333–342. <https://doi.org/10.35234/fumbd.1229068>
38. Wang JJ, Wen ZX, Zhang XH, Zhao YC, Yue ZF (2019) Effect mechanism and equivalent model of surface roughness on fatigue behavior of nickel-based single crystal superalloy. *Int J Fatigue* 125:101–111. <https://doi.org/10.1016/j.ijfatigue.2019.03.041>
39. Lian HS, Chen D, Wang L (2021) Optimization of EDM parameters of insulated ceramic Al₂O₃ using grey relational analysis method. *Electromach Mould* 359(S1):35–39. <https://doi.org/10.3969/j.issn.1009-279X.2021.z1.008>
40. Wang PG, Wang XQ, Liu ZF, Wang HJ, Fu HR (2022) Optimization of process parameters of ultrasonic rolling extrusion based on grey correlation analysis method. *J Plast Eng* 29(3):36–43. <https://doi.org/10.3969/j.issn.1007-2012.2022.03.005>

Publisher's Note Springer Nature remains neutral with regard to jurisdictional claims in published maps and institutional affiliations.

Springer Nature or its licensor (e.g. a society or other partner) holds exclusive rights to this article under a publishing agreement with the author(s) or other rightsholder(s); author self-archiving of the accepted manuscript version of this article is solely governed by the terms of such publishing agreement and applicable law.